



Published in final edited form as:

Med Image Anal. 2015 May ; 22(1): 22–34. doi:10.1016/j.media.2014.12.008.

Patient-Specific Biomechanical Model as Whole-Body CT Image Registration Tool

Mao Li^a, Karol Miller^{a,b}, Grand Roman Joldes^a, Barry Doyle^{c,d}, Revanth Reddy Garlapati^a, Ron Kikinis^e, and Adam Wittek^{a,*}

^aIntelligent Systems for Medicine Laboratory, School of Mechanical and Chemical Engineering, The University of Western Australia, Crawley, Perth, Australia

^bInstitute of Mechanics and Advanced Materials, Cardiff School of Engineering, Cardiff University, Wales, UK

^cVascular Engineering, Intelligent Systems for Medicine Laboratory, School of Mechanical and Chemical Engineering, The University of Western Australia, Crawley, Perth, Australia

^dCentre for Cardiovascular Science, The University of Edinburgh, Edinburgh, UK

^eSurgical Planning Laboratory, Brigham and Women's Hospital, Harvard Medical School, Boston, MA, USA

Abstract

Whole-body computed tomography (CT) image registration is important for cancer diagnosis, therapy planning and treatment. Such registration requires accounting for large differences between source and target images caused by deformations of soft organs/tissues and articulated motion of skeletal structures. The registration algorithms relying solely on image processing methods exhibit deficiencies in accounting for such deformations and motion. We propose to predict the deformations and movements of body organs/tissues and skeletal structures for whole-body CT image registration using patient-specific non-linear biomechanical modelling. Unlike the conventional biomechanical modelling, our approach for building the biomechanical models does not require time-consuming segmentation of CT scans to divide the whole body into non-overlapping constituents with different material properties. Instead, a Fuzzy C-Means (FCM) algorithm is used for tissue classification to assign the constitutive properties automatically at integration points of the computation grid. We use only very simple segmentation of the spine when determining vertebrae displacements to define loading for biomechanical models. We demonstrate the feasibility and accuracy of our approach on CT images of seven patients suffering from cancer and aortic disease. The results confirm that accurate whole-body CT image registration can be achieved using a patient-specific non-linear biomechanical model constructed without time-consuming segmentation of the whole-body images.

*Corresponding author: Intelligent Systems for Medicine Laboratory, School of Mechanical and Chemical Engineering, The University of Western Australia, Crawley, Perth WA 6009, Australia. adam.wittek@uwa.edu.au.

Keywords

Whole-Body CT; Image Registration; Patient-Specific Biomechanical Model; Non-linear Finite Element Analysis; Fuzzy-C Means; Hausdorff Distance

1 Introduction

Reliable and accurate radiographic image registration that aligns the source and target images is critical for application of medical imaging in cancer diagnosis, therapy planning and treatment (Black et al., 1997; D'Amico et al., 2000; Jenkinson and Smith, 2001; Spicer et al., 2004; Van Sint Jan et al., 2006; Warfield et al., 2005; Zaidi, 2007). A large number of medical image registration algorithms solely relying on image processing methods have been successfully developed over the years (Cao and Ruan, 2007; Jenkinson and Smith, 2001; Sotiras et al., 2013; Wells et al., 1996). Many of them have been demonstrated to be effective for selected organs, such as the brain, breast, prostate and lungs (Goerres et al., 2002; Mattes et al., 2003; Oguro et al., 2011; Rueckert et al., 1999; Warfield et al., 2005). However, it has been also recognised that large differences between the source and target images caused by complex rigid-body motion of articulated bones, skeletal segments and body organs and large deformations of soft tissues associated with whole-body CT/MRI registration are very challenging for such algorithms (Baiker et al., 2007; Li et al., 2008; Martin-Fernandez et al., 2005; Wittek et al., 2007). Despite some successful attempts to improve robustness of registration algorithms (Toews and Wells, 2013) and registration accuracy for selected body segments for limited range of rigid body motion and soft organs/tissues deformation (Mahfouz et al., 2003; Stromqvist et al., 2009), the whole-body CT image registration still remains a largely unsolved problem (Li et al., 2008).

Therefore, patient-specific biomechanical modelling methods that account for the mechanical behaviour of organs/tissues were recommended by many researchers for registration problems involving large differences (deformations) between the source and target images (Al-Mayah et al., 2010; Hopp et al., 2013; Warfield et al., 2002; Wittek et al., 2007). Unlike image-based matching, registration algorithms using biomechanical models do not require selection of specific type of source-to-target image transformation and optimisation of the transformation parameters to maximise a selected similarity measure between the transformed and target images. Instead, they rely on principles of mechanics to compute deformations that transform source image to target image. This ensures plausibility and robustness of the predicted deformations. In particular, patient-specific biomechanical modelling has been successfully used in numerous studies on computing the brain deformations for neuroimage registration (Garlapati et al., 2014; Hu et al., 2007; Ji et al., 2009; Mostayed et al., 2013; Wittek et al., 2010; Xu and Nowinski, 2001).

Challenges to overcome when applying biomechanical modelling for medical image registration include quick and reliable generation of patient-specific computational models, automatic segmentation of radiographic images and efficient solution of the models (Miller, 2011; Miller et al., 2010; Mostayed et al., 2013). To facilitate rapid generation of patient-specific biomechanical models for whole-body CT image registration, we abandon time-

consuming image segmentation that divides the problem domain into non-overlapping constituents with different material properties. Instead, we apply tissue classification based on the Fuzzy C-Means (FCM) algorithm to assign the constitutive properties automatically at integration points of the computation grid (Bezdek et al., 1984; Zhang et al., 2013). This, allows us to generate the patient-specific biomechanical model automatically and rapidly.

In principle, any verified method of non-linear computational mechanics accounting for both geometric and material nonlinearity can be used to solve biomechanical models for computing soft organ/tissue deformations for image registration. Non-linear finite element analysis with either implicit (Allard et al., 2007; Taylor et al., 2008) or explicit (Hu et al., 2007; Joldes et al., 2009b; Miller et al., 2007; Wittek et al., 2007) integration in time domain remains the most commonly used approach. In our previous research, we have developed and verified a suite of efficient algorithms for computing soft tissue deformations in the context of neuroimage registration (Joldes et al., 2009b; Miller et al., 2007; Miller et al., 2011). In this study, we adapt and apply these algorithms in registration of whole-body CT images.

To demonstrate feasibility and accuracy of whole-body CT image registration using the proposed non-linear biomechanical model, we analysed sets of whole-body/torso CT images of seven patients. Deformation within the patient's body to align a source image to target image is predicted using a patient-specific model that relies on Total Lagrangian Explicit Dynamics TLED non-linear finite element algorithm (Joldes et al., 2009b; Miller et al., 2007; Miller et al., 2011). Accuracy of the registration is quantitatively assessed using the Hausdorff distance metric to measure the spatial distance between the corresponding Canny edges in the registered (i.e. deformed using the deformations computed by means of biomechanical model) and target images (Fedorov et al., 2008; Garlapati et al., 2013; Garlapati et al., 2014; Huttenlocher et al., 1993).

This paper is organised as follows: the proposed patient-specific non-linear finite element model and the TLED algorithm are presented in Section 2; the computational results, including accuracy evaluation, are given in Section 3 which is followed by the discussion and conclusions in Section 4.

2 Methods

2.1 CT Image Datasets Used in the Study

As CT carries health hazard due to large radiation doses, there are very strict clinical guidelines limiting the number of situations where acquiring whole-body CT should be considered (Environmental Protection Authority, 2013; American College of Radiology, 2011a; American College of Radiology, 2011b). Therefore, we created a challenging test-bed for our registration method not through registration of a large number of image datasets, but by applying them to image datasets for different diseases/pathologies: cancer (Cases II-V in Fig. 1) and aortic diseases (Cases VI and VII in Fig. 1). Each of the analysed datasets consists of two sets of images of a given patient acquired at different times. We treated one of them as moving/source image and another as a target image (Fig. 1 shows sagittal sections for each dataset).

Case I is from the publicly available Slicer Registration Library (Case #20: Intra-subject whole-body/torso PET-CT (http://www.na-mic.org/Wiki/index.php/Projects:RegistrationLibrary:RegLib_C20b). The Slicer Registration Library contains no information about a pathology type for Case I. The CT image datasets of cancer patients (Cases II, III, IV and V) were obtained from the National Biomedical Image Archive (<https://public.cancerimagingarchive.net/ncia/login.jsf>) — freely available to browse, download and use for commercial, scientific and educational purpose under the Creative Commons Attribution 3.0 Unported Licence.

Case VI is from the University Hospital Limerick, Ireland, and CT scan data was acquired for surgical planning and treatment of abdominal aortic aneurysm. Case VII was acquired at the Fremantle Hospital, Australia, with scans taken as part of type B aortic dissection diagnosis and treatment. Local ethics approval was obtained from both institutions. All imaging datasets were anonymous and not acquired specifically for this study.

The CT datasets used in this study were acquired in different resolutions (Table 1). Before conducting the analysis, we resampled them to a common resolution of 1 mm x 1 mm x 2.5 mm. Resampling was conducted using linear interpolation — we applied the “Resample Scalar Volume” procedure in 3DSlicer open source software package for medical image computing (Fedorov et al., 2012).

2.2 Patient-Specific Non-Linear Biomechanical Model

Biomechanics-based medical image registration requires incorporation of patient-specific data in the biomechanical model. However, how to generate biomechanical model quickly and reliably remains unsolved (Miller et al., 2011). A set of methods employed in this study can be regarded as one possible solution to this problem.

2.2.1 Element Type, Geometry and Mesh Generation for Patient-Specific Biomechanical Model

Element Type Selection: In practice, in computational biomechanics tetrahedral elements are often used for spatial discretisation of the problem domain due to availability of automatic mesh generators for complex geometries of the body organs (Irving et al., 2006; Wittek et al., 2007). However, a 4-noded tetrahedral element has an intrinsic drawback of volumetric locking for incompressible or nearly incompressible materials such as soft tissues (Hughes, 2000). Therefore, we used under-integrated (with one Gauss point) 8-noded hexahedral elements that do not exhibit locking (Flanagan and Belytschko, 1981; Irving et al., 2006). Practical aspects of application of hexahedral elements in biomechanical models include preventing of instabilities due to zero energy (hourglass) modes and ensuring the element quality (Yang and King, 2011). For hourglass control, we used the method proposed by Joldes et al. (2008). The efficiency and effectiveness of this method has been verified through application in the studies on computation of brain deformation for neuroimage registration (Joldes et al., 2009b; Wittek et al., 2010). Although no commonly accepted specific guidelines regarding the required quality of hexahedral meshes in biomechanics are available, several authors have formulated their experience-based recommendations (Ito et al., 2009; Mostayed et al., 2013; Shepherd and Johnson, 2009; Yang and King, 2011).

Following Ito et al. (2009), Shepherd and Johnson (2009) and Yang and King (2011), we used element Jacobian and warpage to assess mesh quality. We regarded hexahedral elements with Jacobian below 0.2 as unacceptable poor quality and elements with Jacobian between 0.2 and 0.3 – as questionable quality. In all models used in this study, the element Jacobian was above 0.35 and maximum warpage was 25.

Patient-Specific Geometry: The 3D patient-specific torso geometry was created from the CTs using the 3D SLICER (<http://www.slicer.org/>), an open-source software for visualisation, registration, segmentation and quantification of medical data developed by Artificial Intelligence Laboratory of Massachusetts Institute of Technology and Surgical Planning Laboratory at Brigham and Women’s Hospital and Harvard Medical School. Geometry creation involved application of automated level tracing algorithm available in 3D SLICER to distinguish the patient’s body from the rest of the image and creation of the 3D discrete representation (surface model) of the patient’s body. Internal organs, muscles, fat and other tissues were not segmented.

Patient-Specific Mesh Generation: 3D surface model of the patient’s body was used as the boundary for volumetric discretisation (meshing) using hexahedral elements. Hexahedral mesh was created using IA-FEMesh (a freely available software toolkit for hexahedral mesh generation developed at the University of Iowa) (Grosland et al., 2009) (<http://www.ccad.uiowa.edu/MIMX/projects/IA-FEMesh>) and Hyper Mesh™ (a high-performance commercial finite element mesh generator by Altair, Ltd. of Troy, MI, USA). The maximum element size was designated a value of 5 mm (the maximum voxel in the analysed CTs). However, due to differences in body dimension between the patients, the generated meshes appreciably vary in size (as measured by the number of nodes and elements) as indicated in Fig. 2 and Table 2.

As we used Fuzzy C-Means (FCM) algorithm for tissue classification to assign the constitutive properties automatically at integration points, there was no need to distinguish internal organs when constructing the meshes (Fig. 2).

2.2.2 Load and Boundary Conditions—As suggested in our previous studies (Miller and Lu, 2013; Miller et al., 2011; Miller et al., 2010), for problems where loading is prescribed as forced motion of boundaries, the unknown deformation field within the domain depends very weakly on the mechanical properties of the continuum. In studies involving application of biomechanical models in image registration, the displacements to define forced motion of the boundaries are typically determined by comparing position of corresponding points in the source and target images (Wittek et al., 2010). Body surface (skin) appears to be one possible source of information to determine such displacements. However, there are only very few features (landmarks) on the skin that can be reliably distinguished in CT images. Therefore, we used the spine (vertebrae) when determining the displacements (between the source and target images) to prescribe forced motion of the boundaries — in CT images vertebrae are easy to distinguish from the surrounding soft tissues and their shape does not change between the images.

For a given vertebra, spatial distance between the source and target position was calculated using rigid registration (a built-in algorithm from 3D SLICER) (Fedorov et al., 2012):

$$D = \begin{pmatrix} x_f \\ y_f \\ z_f \end{pmatrix} - \begin{pmatrix} x_m \\ y_m \\ z_m \end{pmatrix} = (R - I) * \begin{pmatrix} x_m \\ y_m \\ z_m \end{pmatrix} + T \quad (1)$$

where D is the distance vector between two corresponding points in the source and target images: $P_m(x_m, y_m, z_m)$ in the source (moving) image and $P_f(x_f, y_f, z_f)$ in the target (fixed) image. R is the rotation transformation, T is the translation transformation and I is a diagonal (identity) matrix.

For the seven CT image sets analysed in this study, the magnitude of the distance vector between the vertebrae in source and target images ranged from 19 mm to 21 mm.

When conducting the registration, the body surface (skin) was allowed to move freely without any contact conditions and constraints. Our method, however, allows for adding correspondence between easily distinguishable surface points as constraints if desirable.

2.2.3 Material Properties—As stated in Section Load and Boundary Conditions, our previous studies (Miller and Lu, 2013; Miller et al., 2011) suggest that for problems where loading is prescribed as forced motion of boundaries, results of computation of (unknown) deformation field within the domain depend very weakly on the mechanical properties of the continuum. However, given large tissue deformations between the source and target images and overwhelming experimental evidence that soft tissues behave like hyperelastic/hyperviscoelastic continua (Bilston et al., 2001; Estes and J.H., 1970; Farshad et al., 1999; Fung, 1993; Jin et al., 2013; Miller, 2000; Miller and Chinzei, 1997, 2002; Pamidi and Advani, 1978; Prange and Margulies, 2002; Snedeker et al., 2005; Snedeker, 2005), a constitutive model compatible with finite deformation solution procedures is needed. Therefore, following Miller et al. (2011) we used the Neo-Hookean hyperelastic model — the simplest constitutive model that satisfies this requirement.

$${}^t_0S = \mu J^{-2/3} \left(I_3 - \frac{1}{3} I_0^t C^{-1} \right) + k(J - 1) J_0^t C^{-1} \quad (2)$$

where t_0S is the second Piola-Kirchhoff stress, μ is the shear modulus, k is the bulk modulus, J is the determinant of the deformation gradient, I is the first invariant of the deviatoric Right Cauchy Green deformation tensor C (the first strain invariant), and I_3 is the identity matrix.

Despite recent progress in magnetic resonance (MR) and ultrasound elastography (Kwah et al., 2012), there is no reliable non-invasive method to determine constitutive properties of human soft tissues in-vivo (Miller and Lu, 2013). Therefore, we adapted a method for tissue classification and material properties assignment based on the Fuzzy C-Means (FCM) algorithm. This method has been successfully used in our previous study for computation of the brain deformations due to craniotomy-induced brain shift (Zhang et al., 2013). The study by Zhang et al. (2013) indicated less than 1 mm differences between the organ deformations

predicted using the model relying on tissue classification based on the FCM algorithm and model with detailed representation of anatomical structures determined through tedious segmentation. A key step in implementation of the FCM algorithm for whole-body tissue classification is to determine the relationship between types/classes of tissues depicted in the image and image intensity. For a given number of intensity cluster centres, the FCM algorithm divides the image intensity into different groups by computing the membership functions that link the intensity at each pixel with all the specified cluster centres (Bezdek et al., 1984; Zhang et al., 2013).

$$J_{FCM} = \sum_{i=1}^N \sum_{j=1}^C u_{ij}^q d(x_i, \theta_j) \quad (3)$$

Where N is data samples (i.e. pixels in CT images), C is the number of cluster centres (tissue types/classes), q is the weighting factor referred to in the literature (Balafar et al., 2010) as the fuzziness degree of clustering, u_{ij} is the fuzzy membership function that expresses the probability of one data sample x_i (pixel) belonging to a specified cluster centre θ_j (tissue class), and d is the spatial distance between data sample x_i and cluster centre θ_j . We used the fuzziness degree of clustering q of 2 which is a value commonly applied for soft tissue classification (Hall et al., 1992; Pham and Prince, 1999).

Following Pohle and Toennies (2001) and Balafar et al. (2010), we calculated the membership functions u_{ij} at each cluster centre θ_j using the following formula

$$u_{ij} = \frac{1}{\sum_{k=1}^C \left(\frac{d(x_i, \theta_j)}{d(x_i, \theta_k)} \right)^{\frac{2}{q-1}}} \quad (4)$$

where

$$\theta_j = \frac{\sum_{i=1}^N u_{ij}^q x_i}{\sum_{i=1}^N u_{ij}^q} \quad (5)$$

and $d(x_i, \theta_j)$ is the Euclidean distance $d^2(x_i, \theta_j) = \|x_i - \theta_j\|^2$ between the data point x_i and cluster centre θ_j . For the image datasets analysed in this study, the minimum was achieved within 100 iterations.

FCM algorithm minimises the objective function J_{FCM} (see Eq. 3) by updating of the membership function u_{ij} and centres of clusters. θ_j For the image datasets analysed in this study, the minimum was achieved within 100 iterations.

The only parameter that has to be selected by the analyst in Equation (3)–(5) is the number of cluster centres C . Detailed explanation of how this parameter was selected for the image datasets analysed in this study is given in *Section 3.1*.

2.3 Numerical Solution

We used Total Lagrangian Explicit Dynamics (TLED) algorithm proposed by Miller et al. (2007) with dynamic relaxation to improve rate of convergence to the steady state solution (Joldes et al., 2009a). This algorithm refers all variables to the original configuration, i.e. the second Piola-Kirchoff stress and Green-Lagrange strain are used. The advantage is that all the derivatives with respect to spatial coordinates can be pre-computed. Another important feature of the TLED algorithm is that it utilises central difference method to discretise the temporal derivatives so that the discretised equations are integrated in stepping forward manner without any iteration. Detailed description of the TLED-based suite of finite element procedures used in this study is given in Joldes et al. (2009a, b) and Miller et al. (2007). These procedures rely on explicit integration in time domain and can be easily parallelised to harness computational power of Graphics Processing Units (GPUs) as shown in Joldes et al. (2010).

2.4 Evaluation of the Registration Accuracy

2.4.1 Qualitative Evaluation—Following Garlapati et al. (2014) and Mostayed et al. (2013), we qualitatively compared the contours/edges automatically detected using Canny edge (Canny, 1986; Li et al., 2013; Mostayed et al., 2013) filter in the registered (i.e. source image warped using the deformations predicted by means of a biomechanical model) and target images.

2.4.2 Quantitative Evaluation—Following our previous studies, edge-based Hausdorff distance (HD) metric (on consistent edges detected using Canny filter) is used here to objectively measure the spatial misalignment between the registered (warped using the deformations predicted by means of a biomechanical model) and target images (Canny, 1986; Garlapati et al., 2013; Garlapati et al., 2014; Mostayed et al., 2013):

$$H(X, Y) = \max(h(X, Y), h(Y, X)) \quad (6)$$

and

$$\begin{aligned} h(X, Y) &= \max_{x \in X} \min_{y \in Y} h'(x, y) \\ h'(x, y) &= \max(h''(x, y), h''(y, x)) \\ h''(x, y) &= \max_{x' \in X} \min_{y' \in Y} \|x' - y'\| \end{aligned} \quad (7)$$

where $X = \{x_1, x_2, \dots, x_m\}$ and $Y = \{y_1, y_2, \dots, y_n\}$ are the consistent (i.e. depicting the same anatomical features) Canny edges in the deformed (registered) and target image respectively. $x = \{x'_1, x'_2, \dots, x'_p\}$ and $y = \{y'_1, y'_2, \dots, y'_l\}$ are the point sets that contain the consistent points from two consistent edges. Operator $\| \cdot \|$ represents the calculation of direct distance between two points as used in the point-based HD metric (Huttenlocher et al., 1993).

From Equation (7) we construct percentile edge-based Hausdorff distance (Garlapati et al., 2013; Mostayed et al., 2013):

$$H_p(X, Y) = P^{th} [\arg \min \|x - y\|_2] \quad (8)$$

Following Garlapati et al. (2014) and Mostayed et al. (2013), we do not report here a single Hausdorff distance value, (Equation 6), but use Equation (8) to report Hausdorff distance values for different percentiles. A plot of the Hausdorff distance values for different percentiles (see *Section 3.2.1*) immediately reveals the percentage of edges that have acceptable misalignment errors. Following Mostayed et al. (2013), two-times the voxel size of the original CT image was regarded here as an acceptable error.

3 Results

3.1 Selection of Cluster Centres for Tissue Classification

With exception of our preliminary analysis of a single CT scan set (Li et al., 2014), there have been no attempts to apply FCM tissue classification for biomechanical models for whole-body CT registration. Therefore, there are no guidelines regarding the number of tissue types (intensity cluster centres) (Fig. 3) that need to be distinguished to achieve desired registration accuracy. Below, we explain, how we determined the number of tissue types (cluster centres) for the Fuzzy C-Means FCM algorithm for seven CT datasets used in this study.

One may expect that bones, muscles, fat, lungs, kidneys, heart, blood vessels and other abdominal organs (including liver, stomach/intestines) need to be distinguished in biomechanical models for computing the deformation for whole body CT registration. Bones and fat can be easily identified as they have distinctive image intensity (Fig. 3). On the other hand, the intensity of muscles, liver and kidneys is similar. Consequently, the FCM algorithm (solely based on image intensity) would classify them as belonging to the same tissue category. There is, however, no drawback as our previous studies on neuroimage registration (Miller and Lu, 2013; Miller et al., 2011; Wittek et al., 2009) suggest that if the loading is prescribed via forced motion of the boundary, the results of computation of deformation field within the domain depend very weakly on the mechanical properties of the analysed continuum.

In the CT scans we analysed in this study, the intensity range for lungs and bones was large, from -1100 to -200 and from 250 to 1100 respectively. Thus, we defined three intensity cluster centres for lungs and two intensity cluster centres for bones. Therefore, when assigning the material properties at the integration point using the FCM algorithm, we distinguished eight tissue classes: 1) Class 1, 2 and 3 for lungs and other gas-filled spaces (such as abdominal cavity); 2) Class 4 for fat; 3) Class 5 for muscles, liver and kidneys; 4) Class 6 for stomach and intestines; and 5) Class 7 and 8 for bones. This resulted in the FCM algorithm with eight intensity cluster centres as indicated in Table 3. The number of tissue classes was kept constant in this study, but the cluster centres have different values for different cases, i.e. the same number of intensity clusters and the different position of the cluster centres were used for all CTs in this study. Table 3 shows the position of cluster centres calculated using FCM algorithm for seven analysed cases.

Table 4 shows the material property (shear modulus) calculated (Alcaraz et al., 2003; Bensamoun et al., 2011; Collinworth et al., 2002; Gennisson et al., 2010; Samani et al., 2007; Watters et al., 1985) at class centres defined in Table 3 for all seven analysed cases, and an example of applying the FCM algorithm to assign the material properties (shear modulus) at the integration points of the biomechanical model is shown in Fig. 4a. Comparison of this figure with the corresponding CT slice (Fig. 4b) indicates that, with exception of very few outliers, the shear modulus assigned by the FCM algorithm is consistent with a tissue type depicted in the image at location of the integration points

3.2 Results of Evaluation of the Registration Accuracy

3.2.1 Qualitative Evaluation—As shown in Fig. 5 (column A) and Fig. 6 (column A), for all seven whole-body/torso CT image datasets analysed in this study, large differences in the edge features between the source and target CTs were present. On the other hand, for the registered (i.e. the source images warped using the deformations predicted by biomechanical models) and target images good overlap (with some local misalignment) of edge features was observed (Fig. 5 — column B and Fig. 6 — column B). The overlap tended to be better in the posterior than anterior and lateral image parts. One possible explanation for this tendency can be that the biomechanical models for computing the tissue deformations were loaded by prescribing the vertebrae motion as described in Section 2.2.2.

3.2.2 Quantitative Evaluation—Analysis of Hausdorff Distance (HD) percentile values indicates that for Case I and Case II, the average HD (as presented in Suh et al. (2012)) between the edges in the registered and target images was less than the original (i.e. before resampling) CT image voxel size of 5 mm (Table 1). For none of the analysed cases, the average HD was greater than two times the voxel size (10 mm for Cases I and II, 5 mm for Cases III – VI and 6mm for Case VII) — a value selected here as the allowable misalignment threshold (see section 2.4.2). Using this threshold, it can be concluded from Fig. 7 and Table 5 that 95% of edges were successfully registered for Cases I and II, 85% — for Cases III – VI and 90% for Case VII. For Cases I and II the resolution in sagittal plane was 5 mm, 2.5 mm for Cases III – VI and 3 mm for Case VII.

For all seven analysed CT image datasets, the percentile edge-based HD curves tend to rise steeply around 95th percentile (Fig. 7). Therefore, it can be suggested that most edge pairs that lie between 96th and 100th percentile are possible outliers as they do not have any correspondence (i.e. edges in the source/registered and target images do not correspond to each other).

No differences in the registration accuracy were observed between the datasets obtained from patients suffering from cancer (Cases II-V) and aortic disease (Cases VI and VII), (Table 5). This confirms feasibility and accuracy of our approach for patients suffering from different diseases.

4 Discussion and Conclusions

In this study, a comprehensive patient-specific non-linear finite element model is proposed for computing the deformations within the patient's body for registration of whole-body CT

images. The proposed approach accounts for rigid body motion of bones/skeletal segments, large deformations, and non-linear constitutive properties of soft tissues. The most commonly used approach for generating patient-specific finite element models involves image segmentation to divide the human body into non-overlapping constituents with different material properties — a very tedious and time consuming process. Therefore, we replaced segmentation with the Fuzzy C-Means algorithm to quickly and automatically classify the tissues and assign the mechanical properties directly at the integration points based on this classification (see section 2.2.3). Therefore, we eliminated the need for body organ/tissue segmentation when constructing biomechanical models for registration of whole-body radiographic images. Selection of ‘fuzzy’ method rather than traditionally used “exact” (i.e. relying on image segmentation) approach to assign the mechanical properties is supported by the fact that when loading is prescribed through forced motion of the boundary (vertebrae motion in this study), the computed deformations are only very weakly sensitive to the mechanical properties of the modelled continuum providing that appropriate algorithms of non-linear computational mechanics are used (Miller, 2005; Miller and Lu, 2013; Wittek et al., 2009).

The feasibility and accuracy of the proposed approach for whole-body CT image registration were verified for CT datasets of seven patients suffering from cancer and aortic disease obtained from publicly available image databases (http://www.na-mic.org/Wiki/index.php/Projects:RegistrationLibrary:RegLib_C20b and <https://public.cancerimagingarchive.net/ncia/login.jsf>) and two hospitals (the University Hospital Limerick, Ireland and the Fremantle Hospital, Australia). Hausdorff Distance HD metric between the corresponding features (Canny edges) in the registered (i.e. source image warped using the deformations predicted by means of a biomechanical model) and target images was used as a quantitative measure of the registration accuracy. The results indicate that for Cases I - VII 85%–95% of edge pairs were registered with an error within two times the voxel size which is a criterion of successful registration used in the literature (Mostayed et al., 2013). However, some local misalignments are clearly visible in Fig. 5 and Fig. 6. One possible source of these misalignments can be that we used very sparse information (vertebrae displacements between the source and target images) to define the model loading. Although one may argue that providing more information to drive computation of the organ and tissue deformations may improve the registration accuracy, the overall results are very promising. It should be noted that to define forced motion of the boundary we relied on simple segmentation of the spine to determine vertebrae displacements between the source and target images.

The present study can be regarded as a pioneering effort to solve challenging problem of whole-body CT image registration by applying a biomechanical model using non-linear finite element procedures to compute the deformations to warp a source image to the patient’s target geometry. For all the analysed image sets, the average Hausdorff distance between the pairs edges in registered and target images was within two times the voxel size, which compares well with the studies on non-rigid registration of whole-body CTs relying solely on image-processing algorithms. For instance, Suh et al. (2012) reported the maximum-likelihood HD (M-HD) of an order of 4 image voxels in their study for rat whole-body CT non-rigid registration using a weighted demons algorithm. Similarly, Toews and Wells (2013) observed errors of an order of 6 image voxel when applying their feature-

based alignment (FBA) method for inter-subject registration of human whole-body CT images.

Acknowledgments

The first author is a recipient of the SIRF scholarship and acknowledges the financial support of the University of Western Australia. The financial support of National Health and Medical Research Council (Grant No. APP1006031) and Australian Research Council (Discovery Grant DP120100402) is gratefully acknowledged. This investigation was also supported in part by NIH grants R01 EB008015 and R01 LM010033, and by a research grant from the Children's Hospital Boston Translational Research Program. In addition, the authors also gratefully acknowledge the financial support of National Centre for Image Guided Therapy (NIH U41RR019703) and the National Alliance for Medical Image Computing (NAMIC), funded by the National Institutes of Health through the NIH Roadmap for Medical Research, Grant U54 EB005149. Information on the National Centres for Biomedical Computing can be obtained from <http://nihroadmap.nih.gov/bioinformatics>. We would also like to thank Paul Norman (at The University of Western Australia and Fremantle Hospital), Eamon Kavanagh and Pierce Grace (at the University Hospital Limerick) for providing some of the CT datasets used in the study. NHMRC Project Grant (GNT1063986) and Career Development Fellowship (GNT1083572) are also gratefully acknowledged.

References

- Al-Mayah A, Moseley J, Hunter S, Velec M, Chau L, Breen S, Brock K. Biomechanical-based image registration for head and neck radiation treatment. *Physics in medicine and biology*. 2010; 55:6491–6500. [PubMed: 20959687]
- Alcaraz J, Buscemi L, Grabulosa M, Trepas X, Fabry B, Farre R, Navajas D. Microrheology of human lung epithelial cells measured by atomic force microscopy. *Biophys J*. 2003; 84:2071–2079. [PubMed: 12609908]
- Allard, J.; Cotin, S.; Faure, F.; Bensoussan, P.-J.; Poyer, F.; Duriez, C.; Delignette, H.; Grisoni, L. SOFA - an open source framework for medical simulation, *Medicine Meets Virtual Reality (MMVR 15)*. CA, USA: Long Beach; 2007. p. 1-6.
- Baiker M, Milles J, Vossepoell AM, Que I, Kaijzel EL, Lowik CWGM, Reiber JHC, Dykstra J, Lelieveldt BPF. Fully automated whole-body registration in mice using an articulated skeleton atlas. *I S Biomed Imaging*. 2007:728–731.
- Balafar MA, Ramli AR, Saripan MI, Mashohor S. Review of brain MRI image segmentation methods. *Artif Intell Rev*. 2010; 33:261–274.
- Bensamoun SF, Robert L, Leclerc GE, Debernard L, Charleux F. Stiffness imaging of the kidney and adjacent abdominal tissues measured simultaneously using magnetic resonance elastography. *Clin Imag*. 2011; 35:284–287.
- Bezdek JC, Ehrlich R, Full W. Fcm - the Fuzzy C-Means Clustering-Algorithm. *Comput Geosci*. 1984; 10:191–203.
- Bilston L, Liu Z, Phan-Tiem N. Large strain behaviour of brain tissue in shear: Some experimental data and differential constitutive model. *Biorheology*. 2001; 38:335–345. [PubMed: 11673648]
- Black PM, Moriarty T, Alexander E, Stieg P, Woodard EJ, Gleason PL, Martin CH, Kikinis R, Schwartz RB, Jolesz FA. Development and implementation of intraoperative magnetic resonance imaging and its neurosurgical applications. *Neurosurgery*. 1997; 41:831–842. [PubMed: 9316044]
- Canny J. A Computational Approach to Edge-Detection. *IEEE T Pattern Anal*. 1986; 8:679–698.
- Cao XM, Ruan QQ. A survey on evaluation methods for medical image registration. 2007 IEEE / ICME International Conference on Complex Medical Engineering. 2007; 1–4:718–721.
- Collinsworth AM, Zhang S, Kraus WE, Truskey GA. Apparent elastic modulus and hysteresis of skeletal muscle cells throughout differentiation. *Am J Physiol-Cell Ph*. 2002; 283:C1219–C1227.
- D'Amico AV, Cormack R, Kumar S, Tempany CM. Real-time magnetic resonance imaging-guided brachytherapy in the treatment of selected patients with clinically localized prostate cancer. *J Endourol*. 2000; 14:367–370. [PubMed: 10910153]
- Estes MSJHM. Response of Brain Tissue of Compressive Loading. ASME Paper No. 1970 70-BHF-13.

- Farshad M, Barbezat M, Flüeler P, Schmidlin F, Graber P, Niederer P. Material characterization of the pig kidney in relation with the biomechanical analysis of renal trauma. *J Biomech.* 1999; 32:417–425. [PubMed: 10213032]
- Fedorov A, Beichel R, Kalpathy-Cramer J, Finet J, Fillion-Robin JC, Pujol S, Bauer C, Jennings D, Fennessy F, Sonka M, Buatti J, Aylward S, Miller JV, Pieper S, Kikinis R. 3D Slicer as an image computing platform for the Quantitative Imaging Network. *Magn Reson Imaging.* 2012; 30:1323–1341. [PubMed: 22770690]
- Fedorov A, Billet E, Prastawa M, Gerig G, Radmanesh A, Warfield SK, Kikinis R, Chrisochoides N. Evaluation of Brain MRI Alignment with the Robust Hausdorff Distance Measures. *Lect Notes Comput Sc.* 2008; 5358:594–603.
- Flanagan DP, Belytschko T. A uniform strain hexahedron and quadrilateral with orthogonal hourglass control. *Int J Numer Methods Eng.* 1981; 17:679–706.
- Fung, YC. *Biomechanics. Mechanical Properties of Living Tissues.* Second ed.. New York: Springer-Verlag; 1993. p. 392-426.
- Garlapati, R.; Joldes, GR.; Wittek, A.; Lam, J.; Weisenfeld, N.; Hans, A.; Warfield, S.; Kikinis, R.; Miller, K. Objective Evaluation of Accuracy of Intra-Operative Neuroimage Registration. In: Wittek, A.; Miller, K.; Nielsen, PMF., editors. *Computational Biomechanics for Medicine: Methods, Algorithms and Implementation.* New York: Springer; 2013. p. 87-99. ISBN 978-1-4614-6350-4
- Garlapati RR, Roy A, Joldes GR, Wittek A, Mostayed A, Doyle B, Warfield SK, Kikinis R, Knuckey N, Bunt S, Miller K. More accurate neuronavigation data provided by biomechanical modeling instead of rigid registration. *J Neurosurg.* 2014; 120:1477–1483. [PubMed: 24460486]
- Gennisson, JL.; Grenier, N.; Hubrecht, R.; Couzy, L.; Delmas, Y.; Derieppe, M.; Lepreux, S.; Merville, P.; Criton, A.; Bercoff, J.; Tanter, M. Multiwave technology introducing shear wave elastography of the kidney: Pre-clinical study on a kidney fibrosis model and clinical feasibility study on 49 human renal transplants, *Ultrasonics Symposium (IUS), 2010 IEEE.* CA: San Diego; 2010. p. 1356-1359.
- Goerres GW, Kamel E, Heidelberg TNH, Schwitter MR, Burger C, von Schulthess GK. PET-CT image co-registration in the thorax: influence of respiration. *Eur J Nucl Med Mol I.* 2002; 29:351–360.
- Grosland NM, Shivanna KH, Magnotta VA, Kallemeyn NA, DeVries NA, Tadepalli SC, Lisle C. IA-FEMesh: An open-source, interactive, multiblock approach to anatomic finite element model development. *Computer Methods and Programs in Biomedicine.* 2009; 94:96–107. [PubMed: 19157630]
- Hall LO, Bensaid AM, Clarke LP, Velthuizen RP, Silbiger MS, Bezdek JC. A Comparison of Neural Network and Fuzzy Clustering-Techniques in Segmenting Magnetic-Resonance Images of the Brain. *IEEE T Neural Networ.* 1992; 3:672–682.
- Hopp T, Dietzel M, Baltzer PA, Kreisel P, Kaiser WA, Gemmeke H, Ruitter NV. Automatic multimodal 2D/3D breast image registration using biomechanical FEM models and intensity-based optimization. *Med Image Anal.* 2013; 17:209–218. [PubMed: 23265802]
- Hu J, Jin X, Lee Jb, Zhang L, Chaudhary V, Guthikonda M, Yang KH, King AI. Intraoperative brain shift prediction using a 3D inhomogeneous patient-specific finite element model. *Journal of Neurosurgery.* 2007; 106:164–169. [PubMed: 17236503]
- Hughes TJR. *The Finite Element Method: Linear Static and Dynamic Finite Element Analysis.* Dover Publications, Mineola. 2000
- Huttenlocher DP, Klanderman GA, Rucklidge WJ. Comparing Images Using the Hausdorff Distance. *IEEE T Pattern Anal.* 1993; 15:850–863.
- Irving G, Teran J, Fedkiw R. Tetrahedral and hexahedral invertible finite elements. *Graph Models.* 2006; 68:66–89.
- Ito Y, Shih AM, Soni BK. Octree-based reasonable-quality hexahedral mesh generation using a new set of refinement templates. *Int J Numer Methods Eng.* 2009; 77:1809–1833.
- Jenkinson M, Smith S. A global optimisation method for robust affine registration of brain images. *Med Image Anal.* 2001; 5:143–156. [PubMed: 11516708]

- Ji S, Roberts DW, Hartov A, Paulsen KD. Brain-skull contact boundary conditions in an inverse computational deformation model. *Med Image Anal.* 2009; 13:659–672. [PubMed: 19560393]
- Jin X, Zhu F, Mao H, Shen M, Yang KH. A comprehensive experimental study on material properties of human brain tissue. *J Biomech.* 2013; 46:2795–2801. [PubMed: 24112782]
- Joldes GR, Wittek A, Miller K. An efficient hourglass control implementation for the uniform strain hexahedron using the Total Lagrangian formulation. *Commun Numer Meth En.* 2008; 24:1315–1323.
- Joldes GR, Wittek A, Miller K. Computation of intra-operative brain shift using dynamic relaxation. *Comput Method Appl M.* 2009a; 198:3313–3320.
- Joldes GR, Wittek A, Miller K. Suite of finite element algorithms for accurate computation of soft tissue deformation for surgical simulation. *Med Image Anal.* 2009b; 13:912–919. [PubMed: 19152791]
- Joldes GR, Wittek A, Miller K. Real-Time Nonlinear Finite Element Computations on GPU - Application to Neurosurgical Simulation. *Comput Methods Appl Mech Eng.* 2010; 199:3305–3314. [PubMed: 21179562]
- Kwah LK, Herbert RD, Harvey LA, Diong J, Clarke JL, Martin JH, Clarke EC, Hoang PD, Bilston LE, Gandevia SC. Passive Mechanical Properties of Gastrocnemius Muscles of People With Ankle Contracture After Stroke. *Arch Phys Med Rehab.* 2012; 93:1185–1190.
- Li, M.; Wittek, A.; Joldes, G.; Zhang, G.; Dong, F.; Kikinis, R.; Miller, K. Whole-Body Image Registration Using Patient-Specific Non-Linear Finite Element Model. In: Doyle, BJ.; Miller, K.; Wittek, A.; Nielsen, PMF., editors. *Computational Biomechanics for Medicine: Fundamental Science and Patient-Specific Application.* New York: Springer; 2014. p. 21-30. ISBN 978-1-4938-0744-1
- Li X, Yankeelov TE, Peterson TE, Gore JC, Dawant BM. Automatic nonrigid registration of whole body CT mice images. *Med Phys.* 2008; 35:1507–1520. [PubMed: 18491546]
- Mahfouz MR, Hoff WA, Komistek RD, Dennis DA. A robust method for registration of three-dimensional knee implant models to two-dimensional fluoroscopy images. *IEEE T Med Imaging.* 2003; 22:1561–1574.
- Martin-Fernandez MA, Munoz-Moreno E, Martin-Fernandez M, Alberola-Lopez C. Articulated registration: elastic registration based on a wire-model. *Proc Spie.* 2005; 5747:182–191.
- Mattes D, Haynor DR, Vesselle H, Lewellen TK, Eubank W. PET-CT image registration in the chest using free-form deformations. *IEEE T Med Imaging.* 2003; 22:120–128.
- Miller K. Constitutive modelling of abdominal organs. *J Biomech.* 2000; 33:367–373. [PubMed: 10673121]
- Miller K. Biomechanics without mechanics: Calculating soft tissue deformation without differential equations of equilibrium, Symposium on Computer Methods in Biomechanics and Biomedical Engineering, Madrid, Spain. 2005
- Miller, K. *Biomechanics of the brain.* New York: Springer; 2011.
- Miller K, Chinzei K. Constitutive modeling of brain tissue: Experiment and theory. *J Biomech.* 1997; 30:1115–1121. [PubMed: 9456379]
- Miller K, Chinzei K. Mechanical properties of brain tissue in tension. *J Biomech.* 2002; 35:483–490. [PubMed: 11934417]
- Miller K, Joldes G, Lance D, Wittek A. Total Lagrangian explicit dynamics finite element algorithm for computing soft tissue deformation. *Commun Numer Meth En.* 2007; 23:121–134.
- Miller K, Lu J. On the prospect of patient-specific biomechanics without patient-specific properties of tissues. *Journal of the Mechanical Behavior of Biomedical Materials.* 2013; 27:154–66. [PubMed: 23491073]
- Miller, K.; Wittek, A.; Joldes, G. Biomechanical Modeling of the Brain for Computer-Assisted Neurosurgery. In: Miller, K., editor. *Biomechanics of the Brain.* New York: Springer; 2011. p. 111-136.
- Miller K, Wittek A, Joldes G, Horton A, Dutta-Roy T, Berger J, Morriss L. Modelling brain deformations for computer-integrated neurosurgery. *Int J Numer Meth Bio.* 2010; 26:117–138.

- Mostayed A, Garlapati RR, Joldes GR, Wittek A, Roy A, Kikinis R, Warfield SK, Miller K. Biomechanical Model as a Registration Tool for Image-Guided Neurosurgery: Evaluation Against BSpline Registration. *Ann Biomed Eng.* 2013; 41:2409–2425. [PubMed: 23771299]
- Oguro S, Tuncali K, Elhawary H, Morrison PR, Hata N, Silverman SG. Image registration of pre-procedural MRI and intra-procedural CT images to aid CT-guided percutaneous cryoablation of renal tumors. *Int J Comput Ass Rad.* 2011; 6:111–117.
- Pamidi MR, Advani SH. Nonlinear Constitutive Relations for Human Brain Tissue. *Trans. ASME, J. Biomech. Eng.* 1978; 100:44–48.
- Pham DL, Prince JL. Adaptive fuzzy segmentation of magnetic resonance images. *IEEE T Med Imaging.* 1999; 18:737–752.
- Pohle R, Toennies KD. Segmentation of medical images using adaptive region growing. 2001:1337–1346.
- Prange MT, Margulies SS. Regional, directional, and age-dependent properties of the brain undergoing large deformation. *ASME Journal of Biomechanical Engineering.* 2002; 124:244–252.
- Rueckert D, Sonoda LI, Hayes C, Hill DLG, Leach MO, Hawkes DJ. Nonrigid registration using free-form deformations: Application to breast MR images. *IEEE T Med Imaging.* 1999; 18:712–721.
- Samani A, Zubovits J, Plewes D. Elastic moduli of normal and pathological human breast tissues: an inversion-technique-based investigation of 169 samples. *Physics in Medicine and Biology.* 2007; 52:1565–1576. [PubMed: 17327649]
- Shepherd J, Johnson C. Hexahedral mesh generation for biomedical models in SCIRun. *Engineering with Computers.* 2009; 25:97–114.
- Snedeker JG, Barbezat M, Niederer P, Schmidlin FR, Farshad M. Strain energy density as a rupture criterion for the kidney: impact tests on porcine organs, finite element simulation, and a baseline comparison between human and porcine tissues. *J Biomech.* 2005; 38:993–1001. [PubMed: 15797581]
- Snedeker JGG. Strain-rate dependent material properties of the porcine and human kidney capsule. *J Biomech.* 2005; 38:1011–1021. [PubMed: 15797583]
- Sotiras A, Davatzikos C, Paragios N. Deformable Medical Image Registration: A Survey. *IEEE T Med Imaging.* 2013; 32:1153–1190.
- Spicer MA, van Velsen M, Caffrey JP, Apuzzo MLJ. Virtual reality neurosurgery: A simulator blueprint. *Neurosurgery.* 2004; 54:783–797. [PubMed: 15046644]
- Stromqvist B, Fritzell P, Hagg O, Jonsson B, Surg SS. The Swedish Spine Register: development, design and utility. *Eur Spine J.* 2009; 18:S294–S304.
- Suh JW, Kwon OK, Scheinost D, Sinusas AJ, Cline GW, Papademetris X. CT-PET weighted image fusion for separately scanned whole body rat. *Med Phys.* 2012; 39:533–542. [PubMed: 22225323]
- Taylor ZA, Cheng M, Ourselin S. High-Speed Nonlinear Finite Element Analysis for Surgical Simulation Using Graphics Processing Units. *IEEE Transactions on Medical Imaging.* 2008; 27:650–663. [PubMed: 18450538]
- Toews M, Wells WM. Efficient and robust model-to-image alignment using 3D scale-invariant features. *Med Image Anal.* 2013; 17:271–282. [PubMed: 23265799]
- Van Sint Jan S, Sobzack S, Dugailly PM, Feipel V, Lefevre P, Lufimpadio JL, Salvia P, Viceconti M, Rooze M. Low-dose computed tomography: a solution for in vivo medical imaging and accurate patient-specific 3D bone modeling? *Clin Biomech (Bristol, Avon).* 2006; 21:992–998.
- Warfield SK, Haker SJ, Talos IF, Kemper CA, Weisenfeld N, Mewes AUJ, Goldberg-Zimring D, Zou KH, Westin CF, Wells WM, Tempany CMC, Golby A, Black PM, Jolesz FA, Kikinis R. Capturing intraoperative deformations: research experience at Brigham and Women's Hospital. *Med Image Anal.* 2005; 9:145–162. [PubMed: 15721230]
- Warfield SK, Talos F, Tei A, Bharatha A, Nabavi A, Ferrant M, Black PM, Jolesz FA, Kikinis R. Real-time registration of volumetric brain MRI by biomechanical simulation of deformation during image guided neurosurgery. *Computing and Visualization in Science.* 2002; 5:3–11.
- Watters DAK, Smith AN, Eastwood MA, Anderson KC, Elton RA. Mechanical-Properties of the Rat Colon - the Effect of Age, Sex and Different Conditions of Storage. *Q J Exp Physiol Cms.* 1985; 70:151–162.

- Wells WM 3rd, Viola P, Atsumi H, Nakajima S, Kikinis R. Multi-modal volume registration by maximization of mutual information. *Med Image Anal.* 1996; 1:35–51. [PubMed: 9873920]
- Wittek A, Hawkins T, Miller K. On the unimportance of constitutive models in computing brain deformation for image-guided surgery. *Biomech Model Mechan.* 2009; 8:77–84.
- Wittek A, Joldes G, Couton M, Warfield SK, Miller K. Patient-specific non-linear finite element modelling for predicting soft organ deformation in real-time; Application to non-rigid neuroimage registration. *Prog Biophys Mol Bio.* 2010; 103:292–303. [PubMed: 20868706]
- Wittek A, Miller K, Kikinis R, Warfield SK. Patient-specific model of brain deformation: Application to medical image registration. *J Biomech.* 2007; 40:919–929. [PubMed: 16678834]
- Xu M, Nowinski WL. Talairach-Tournoux brain atlas registration using a metalforming principle-based finite element method. *Med Image Anal.* 2001; 5:271–279. [PubMed: 11731306]
- Yang, KH.; King, AI. Modeling of the Brain for Injury Simulation and Prevention. In: Miller, K., editor. *Biol Med Phys Biomed.* New York: Springer; 2011. p. 91-110.
- Zaidi H. Optimisation of whole-body PET/CT scanning protocols. *Biomedical Imaging and Intervention Journal.* 2007; 3:e36. [PubMed: 21614277]
- Zhang JY, Joldes GR, Wittek A, Miller K. Patient-specific computational biomechanics of the brain without segmentation and meshing. *Int J Numer Meth Bio.* 2013; 29:293–308.

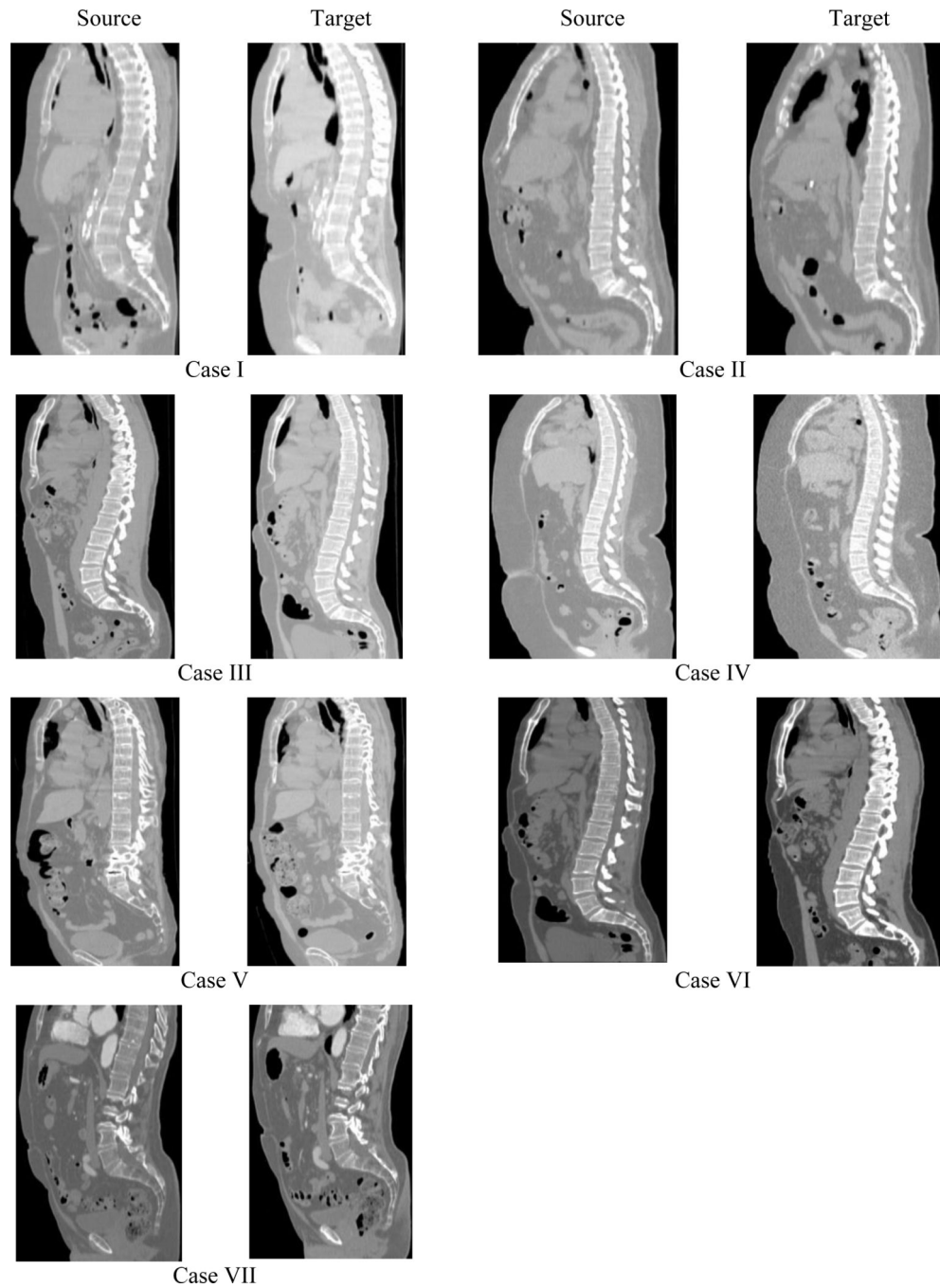


Fig. 1. Sagittal sections of seven CT image datasets analysed in this study. For Case I, no information about the pathology type is available. Cases II-V are patients suffering from cancer. Cases VI and VII are patients suffering from aortic disease.

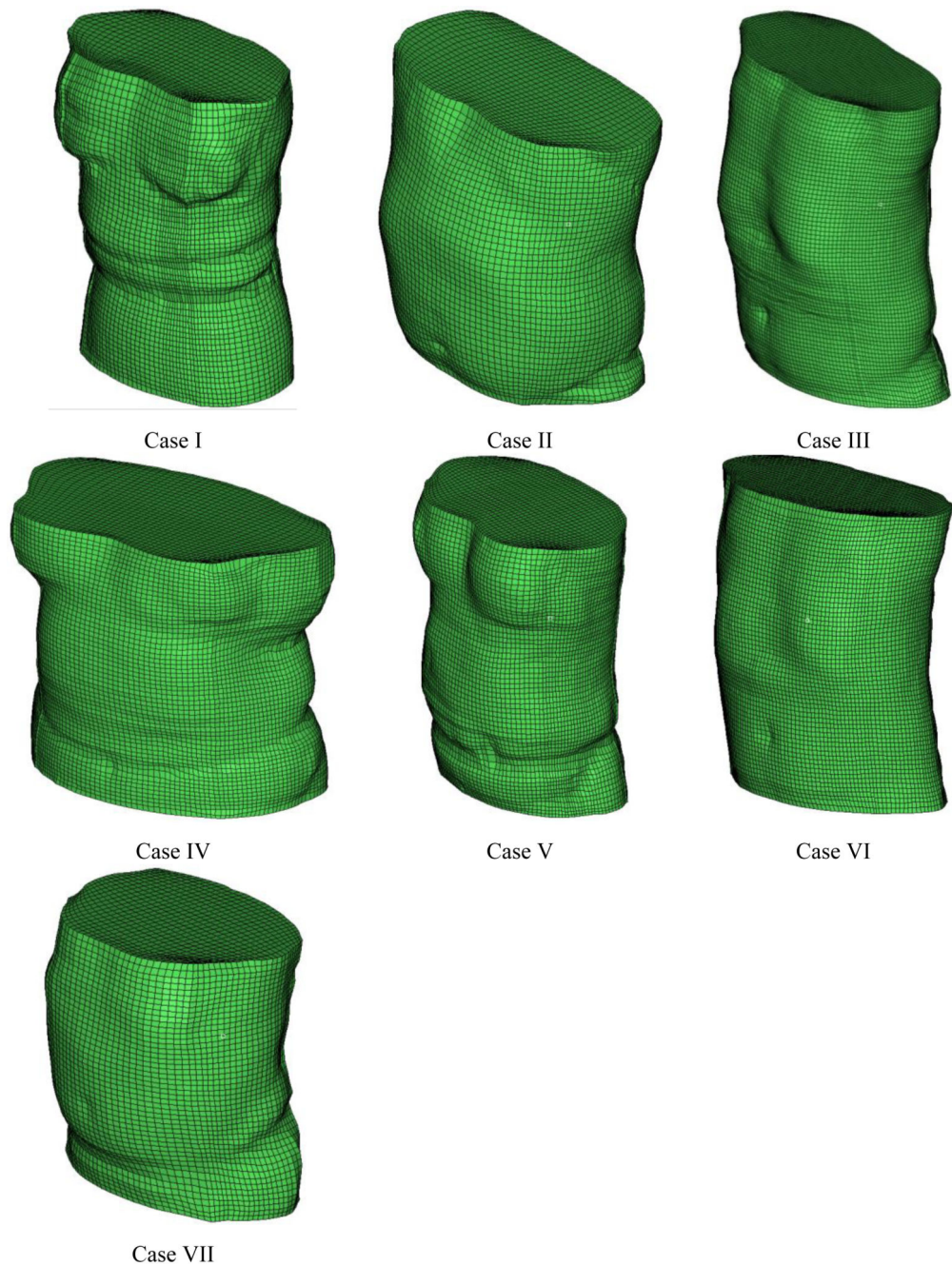
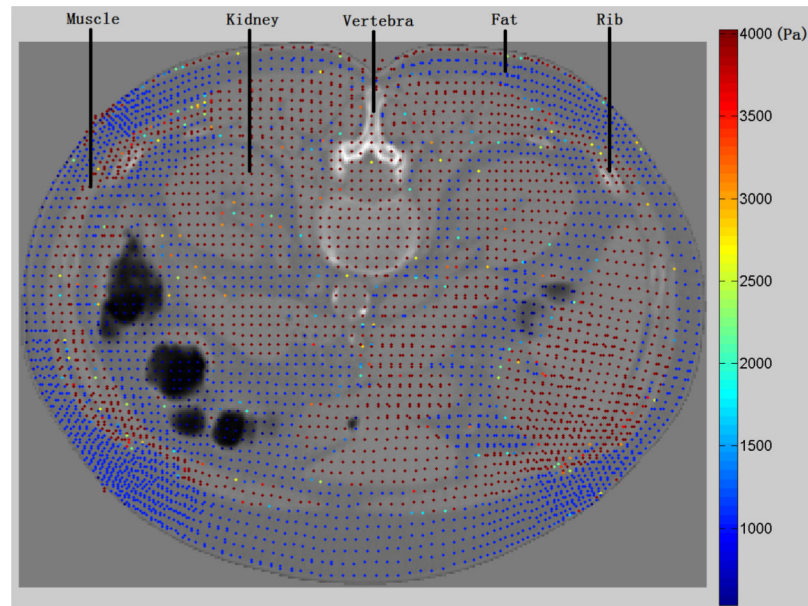


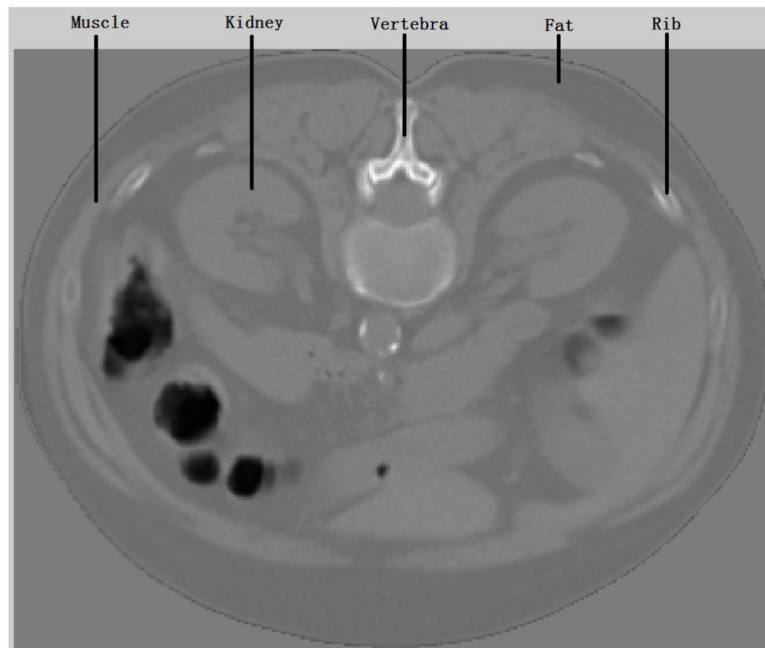
Fig. 2. Patient-specific hexahedral meshes built in this study. We used Fuzzy C-Means (FCM) algorithm for tissue classification to assign the constitutive properties automatically at integration points, there was no need to distinguish internal organs when constructing the meshes.



Fig. 3. Tissue classification for a torso CT transverse section. A certain number of organs/tissues (i.e. bones and fat) can be recognised by distinctive image intensity. Some organs/tissues have similar image intensity (i.e. kidneys, liver, small/large intestines and muscles).



(a)



(b)

Fig. 4. (a) Material properties (shear modulus) assignment for body tissues using FCM algorithm for Case I. Shear modulus magnitude is represented by colour scale. (b) The corresponding CT slice. Note that the points belonging to the same tissue class have similar image intensity and concentrate around the class centre. This can be seen in (a) as a spatial clustering of pixels of the same colour. Only in the boundary areas between different tissue classes, some variation of the pixel colour (shear modulus) occurs.

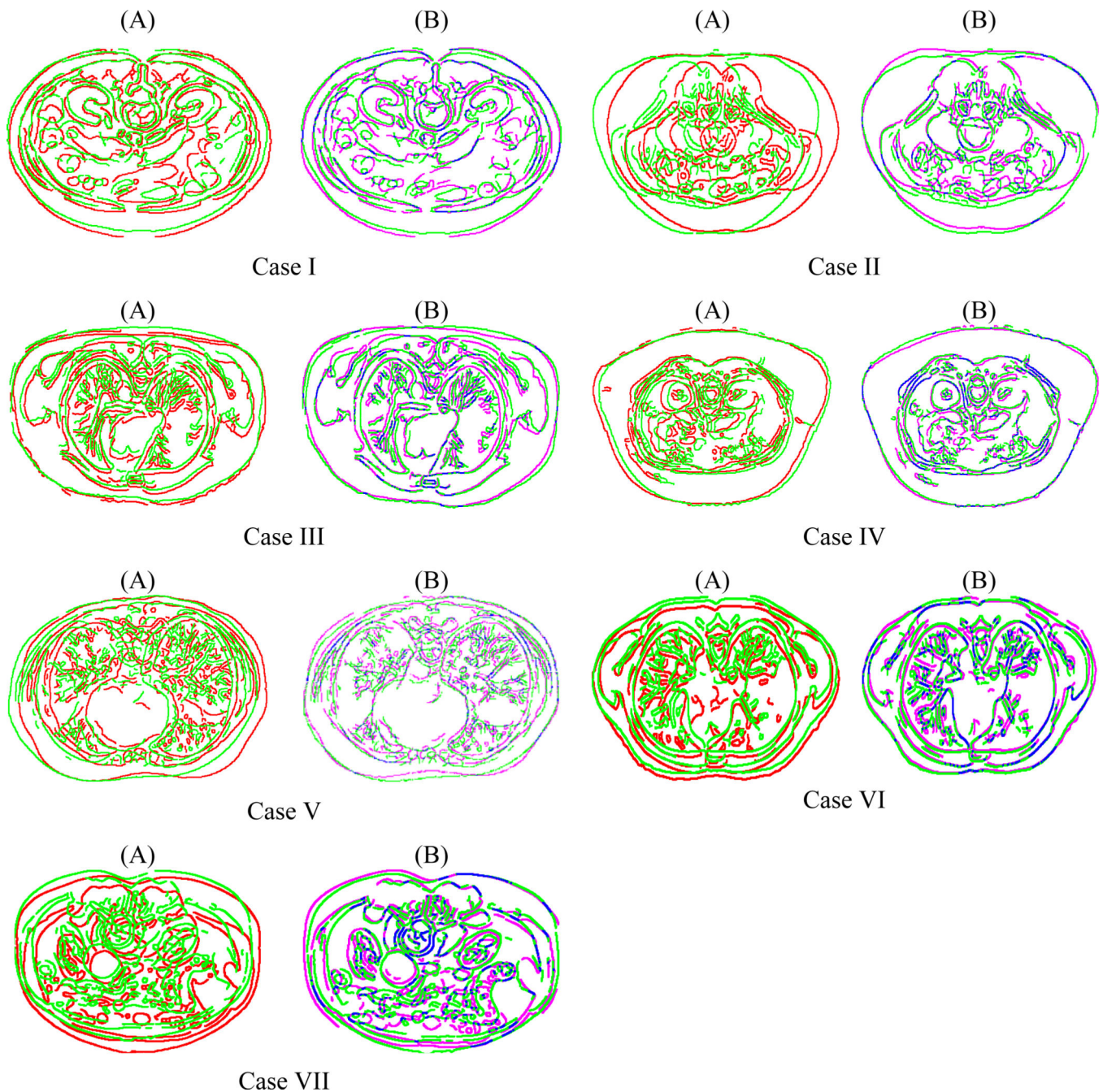


Fig. 5. Qualitative evaluation of the registration accuracy for seven CT image datasets analysed in this study (transverse slices). For each case, (A) comparison of the edges in the source and target image; and (B) — indicates comparison of the edges in the registered (i.e. warped using the deformation computed by biomechanical models developed in this study) and target image. Edges in the source image are indicated by red colour; edges in target image — by green colour; and the edges in the registered image — by pink colour. Good overlap (with some local misalignment) between the edges in registered and target images is evident.

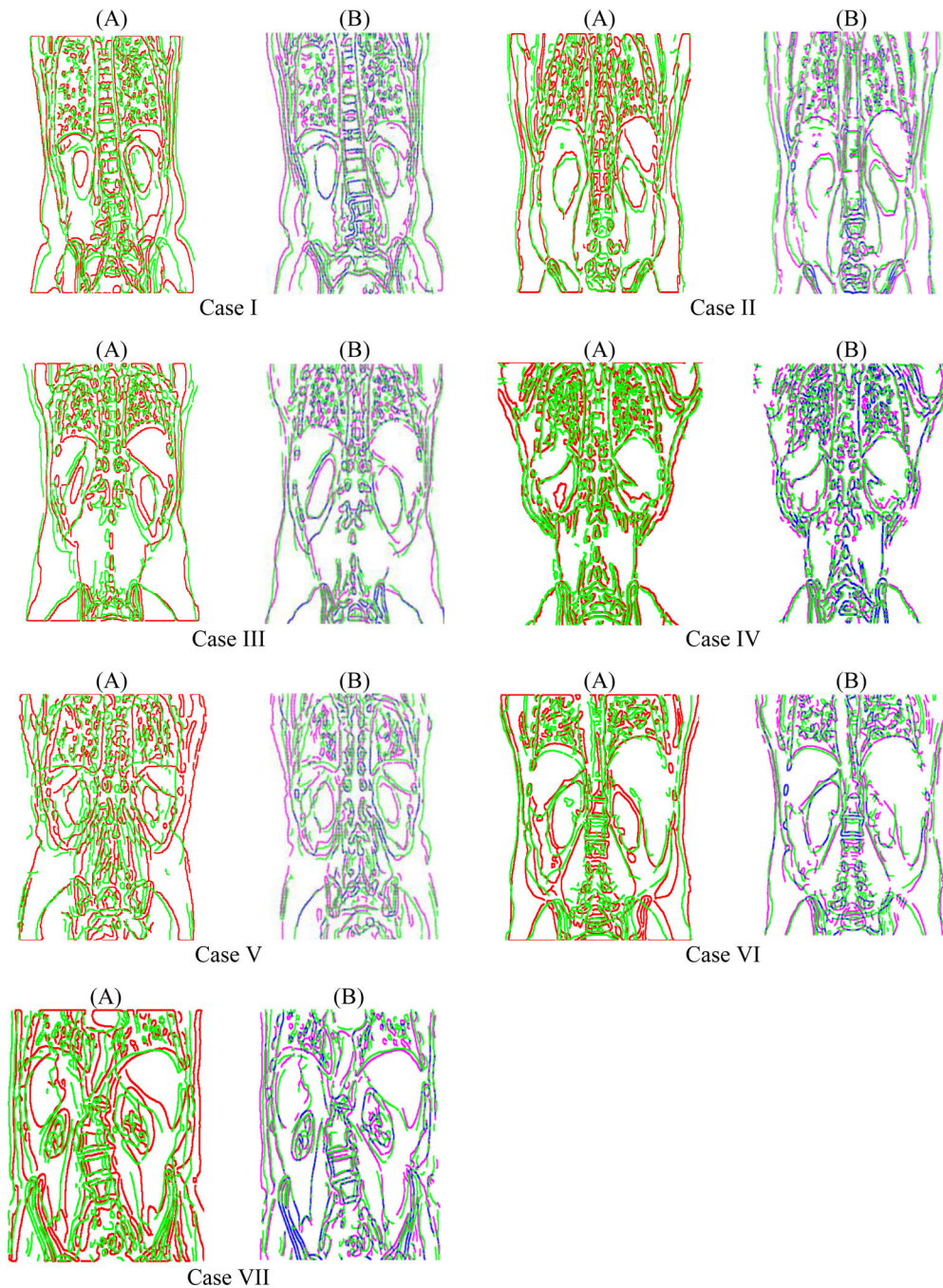


Fig. 6. Qualitative evaluation of the registration accuracy for seven CT image datasets analysed in this study (frontal slices). For each case, (A) comparison of the edges in the source and target image; and (B) — indicates comparison of the edges in the registered (i.e. warped using the deformation computed by biomechanical models developed in this study) and target image. Edges in the source image are indicated by red colour; edges in target image — by green colour; and the edges in the registered image — by pink colour. Good overlap (with some local misalignment) between the edges in registered and target images is evident.

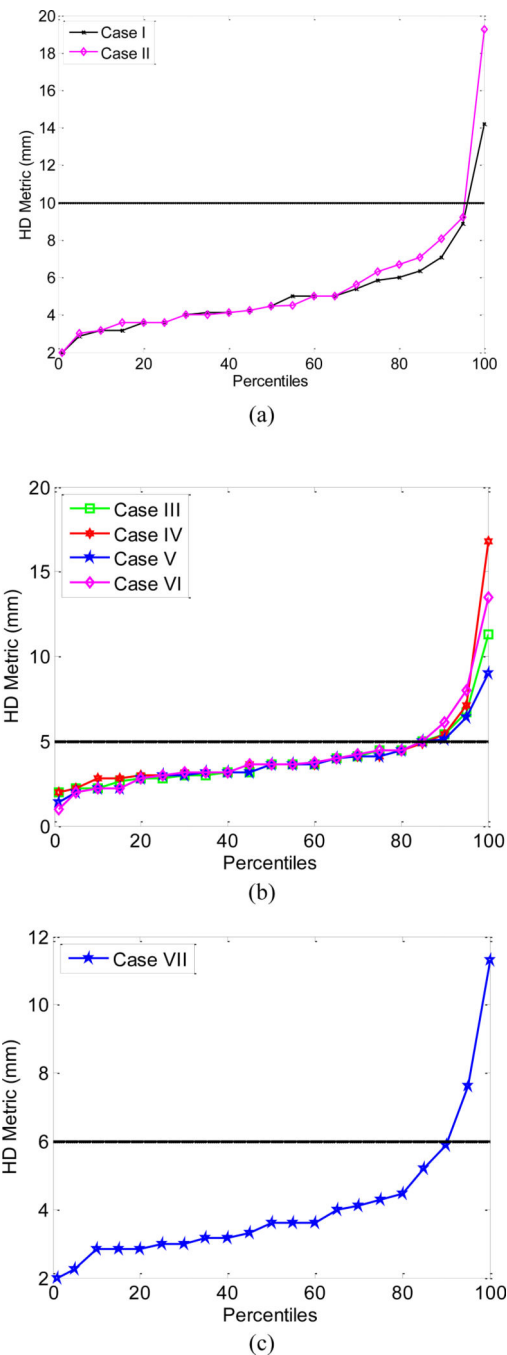


Fig. 7. Quantitative evaluation of the registration accuracy for seven whole-body CT image datasets analysed in this study: edge-based Hausdorff Distance (HD) between the registered (i.e. source images warped using the deformation computed by means of non-linear biomechanical models created in this study) and target images against the percentile of edges for transverse slices. The horizontal line is two times voxel size registration accuracy threshold. Plots for Cases I and II, Cases III–V and Case VII are shown separately due to the differences in image resolution (Cases I and II —sagittal resolution of 5 mm; Cases III–V —

sagittal resolution of 2.5 mm; Case VII— sagittal resolution of 3.0 mm). (a) Cases I and II; (b) Cases III–VI; (c) Case VII.

Author Manuscript

Author Manuscript

Author Manuscript

Author Manuscript

Table 1

Resolution (in mm) of seven CT image datasets analysed in this study

	Source Image (mm)	Target Image (mm)
Case I	0.98×0.98×5.0	0.98×0.98×5.0
Case II	1.00×1.00×5.0	1.00×1.00×5.0
Case III	0.84×0.84×2.5	0.80×0.80×2.5
Case IV	0.90×0.90×2.5	0.98×0.98×2.5
Case V	1.05×1.05×2.5	1.06×1.06×2.5
Case VI	1.00×1.00×2.5	1.00×1.00×2.5
Case VII	0.86×0.86×3.0	0.76×0.76×3.0

Author Manuscript

Author Manuscript

Author Manuscript

Author Manuscript

Table 2

Numbers of hexahedral elements and nodes for seven analysed cases

	Number of Nodes	Number of Elements
Case I	55,944	51,479
Case II	88,265	82,301
Case III	54,190	49,950
Case IV	137,344	128,989
Case V	78,573	72,897
Case VI	86,016	92,625
Case VII	50,889	49,478

Author Manuscript

Author Manuscript

Author Manuscript

Author Manuscript

Table 3

Cluster centres obtained using the FCM algorithm for seven analysed CT image datasets

(8 Classes)	Class 1	Class 2	Class 3	Class 4	Class 5	Class 6	Class 7	Class 8
Case I	-842	-715	-215	-98	-31	29	240	641
Case II	-779	-522	-323	-97	-29	28	245	590
Case III	-826	-537	-326	-90	-32	43	274	661
Case IV	-711	-519	-303	-104	-45	57	253	665
Case V	-650	-481	-247	-89	-38	16	238	527
Case VI	-825	-656	-388	-103	-20	52	219	453
Case VII	-704	-530	-319	-95	-15	61	231	446

Table 4

Shear modulus ($\times 10^3$ Pa) at cluster centres for seven analysed CT image datasets

	Class 1	Class 2	Class 3	Class 4	Class 5	Class 6	Class 7	Class 8
Shear Modulus (kPa)	0.53	0.53	0.53	1.07	3.57	4.02	rigid	rigid
	(Alcaraz et al., 2003)	(Alcaraz et al., 2003)	(Alcaraz et al., 2003)	(Samani et al., 2007)	(Bensamoun et al., 2011; Collinsworth et al., 2002; Gennisson et al., 2010)	(Watters et al., 1985)		

95, 85, 75 and 60 –percentile, average HD metric and voxel size in inferior-superior direction (mm) for the registration accuracy of whole-body CT image of seven cases.

Table 5

	95- Percentile HD metric	85- Percentile HD metric	75- Percentile HD metric	60- Percentile HD metric	Average HD metric	Voxel size in inferior-superior direction
Case I	8.86	6.33	5.83	5.03	4.93	5.0
Case II	9.21	7.07	6.32	5.17	5.20	5.0
Case III	6.70	5.00	4.47	3.64	3.77	2.5
Case IV	7.10	4.86	4.12	3.61	3.90	2.5
Case V	6.39	5.00	4.14	3.60	3.71	2.5
Case VI	8.00	5.00	4.47	3.72	3.64	2.5
Case VII	7.61	5.21	4.30	3.60	3.88	3.0